Relationships of upper tropospheric water vapor, clouds and SST: MLS observations, ECMWF analyses and GCM simulations

Hui Su,[1] Duane E. Waliser,[1] Jonathan H. Jiang,[1] Jui-lin Li,[1] William G. Read,[1] Joe W. Waters,[1] and Adrian M. Tompkins[2]

Received 14 July 2006; revised 8 September 2006; accepted 18 October 2006; published 18 November 2006.

[1] The relationships of upper tropospheric water vapor (UTWV), cloud ice and sea surface temperature (SST) are examined in the annual cycles of ECMWF analyses and simulations from 15 atmosphere-ocean coupled models which were contributed to the IPCC AR4. The results are compared with the observed relationships based on UTWV and cloud ice measurements from MLS on Aura. It is shown that the ECMWF analyses produce positive correlations between UTWV, cloud ice and SST, similar to the MLS data. The rate of the increase of cloud ice and UTWV with SST is about 30% larger than that for MLS. For the IPCC simulations, the relationships between UTWV, cloud ice and SST are qualitatively captured. However, the magnitudes of the simulated cloud ice show a considerable disagreement between models, by nearly a factor of 10. The amplitudes of the approximate linear relations between UTWV, cloud ice and SST vary by a factor up to 4. **Citation:** Su, H., D. E. Waliser, J. H. Jiang, J. Li, W. G. Read, J. W. Waters, and A. M. Tompkins (2006), Relationships of upper tropospheric water vapor, clouds and SST: MLS observations, ECMWF analyses and GCM simulations, *Geophys. Res. Lett.*, *33*, L22802, doi:10.1029/2006GL027582.

1. Introduction

[2] Variabilities of water vapor and clouds are central to global hydrological and energy cycles [e.g., *Pierrehumbert*, 2002; *Held and Soden*, 2000]. The latent heat release associated with phase transitions among gas, liquid and solid forms of water is one of the main modes of energy transport in the atmosphere. Besides their active roles in moist dynamics, water vapor and clouds both have important radiative effects. The greenhouse effect of water vapor increases sharply when temperature increases, leading to a positive feedback for climate change. Clouds can either warm or cool the Earth's surface depending on their height and thickness. They are also intimately related to the distribution of water vapor, especially in the upper troposphere (UT) [*Lindzen*, 1990; *Betts*, 1990; *Sun and Lindzen*, 1993; *Soden and Fu*, 1995; *Udelhofen and Hartmann*, 1995]. Recent satellite observations of UT water vapor (UTWV) and cloud ice water content (IWC) from the Microwave Limb Sounder (MLS) [*Waters et al.*, 2006] on Aura satellite show that UTWV and IWC are positively correlated, and both quantities increase with increasing sea surface temperature (SST) when SST is greater than ~300 K. [*Su et al.*, 2006, hereinafter referred to as SU06]. Over the convective regions, the rate of increase of UTWV with SST is ~3 times larger than that for non-convective regions, largely due to the vertical transport of water vapor by deep convection and re-evaporation of condensates (SU06), although the relative contribution of each process is difficult to determine from the observations alone. This convective enhancement of the greenhouse effect by UTWV explains roughly 65% of the "Super Greenhouse Effect" [*Raval and Ramanathan*, 1989]. SU06 termed the positive correlations of water vapor, clouds and SST as "convective UT water vapor feedback" (CWVF). Note that CWVF refers to the local coupling of UTWV with deep convection and associated clouds, and their connection with the SST gradient: warmer SST favors convection and stronger convection leads to moister UT. However, caution must be exercised when applying the results to long-term climate change. For example, if tropical SSTs were to increase uniformly, with no impact on SST gradients, cloud ice may not increase substantially, or may even decrease [e.g., *Tompkins and Craig*, 1999]. Nevertheless, quantification of the spatial relationships between UTWV, clouds and SST in the present climate is important to understand how cloud and water vapor feedbacks will operate in a future climate with modified SST patterns and gradients.

[3] SU06 provides the first quantitative analysis of relationships between UTWV, IWC and SST using simultaneous direct measurements of UTWV and IWC. It thus serves as a reference point for evaluation of the performance of a state-of-the-art data assimilation model and general circulation models (GCMs) in terms of CWVF. In this paper, we examine to what extent current models capture the relationships of UTWV, cloud ice, and SST and compare them quantitatively with MLS observations. We analyze the European Center for Medium-Range Weather Forecasting model (ECMWF) analyses for the same period as the MLS observations, and the mean annual cycles over the period of 1970 to 1999 from a number of GCMs that were contributed to the Intergovernmental Panel on Climate Change (IPCC) 4th Assessment Report (AR4).

2. ECMWF Analyses

[4] We use the ECMWF analyses from the Integrated Forecasting System (IFS) data assimilation system (DAS) for the period of August 2004 to July 2005, same as that for the MLS data of SU06. The MLS data are not assimilated in the ECMWF model system, ensuring the independence of the two datasets. The ECMWF water vapor and IWC profiles at 00Z, 06Z, 12Z and 18Z are interpolated onto

[1]Jet Propulsion Laboratory, California Institute of Technology, Pasadena, California, USA.
[2]European Center for Medium-Range Weather Forecasts, Reading, UK.

0094-8276/06/2006GL027582$05.00

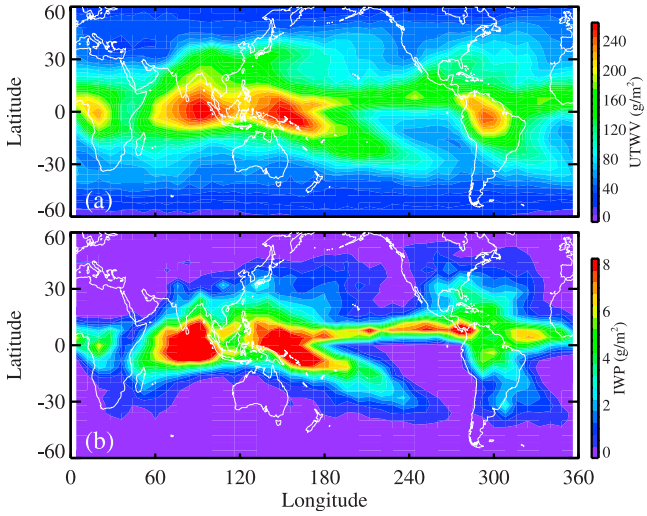

Figure 1. Maps of annual mean ECMWF (a) UTWV (vertically integrated from 316 to 147 hPa) and (b) IWP (vertically integrated IWC from 215 hPa to 147 hPa).

the Aura MLS measurement track in both time and space, as developed and described by J.-L. Li et al. (Assessing consistency between EOS MLS and ECMWF analyzed and forecast estimates of cloud ice, submitted to *Geophysical Research Letters*, 2006, hereinafter referred to as Li et al., submitted manuscript, 2006). Then monthly averages are constructed and horizontal re-griding onto the 8° (longitude) × 4° (latitude) grids is performed, in the same fashion as for MLS data to ensure sampling errors are minimized for comparison.

[5] Figure 1 shows the maps of annual-mean ECMWF UTWV, vertically integrated between 316 and 147 hPa, and cloud ice water path (IWP) integrated between 215 and 147 hPa. The vertical integrals are constructed in exactly the same way as done by SU06 for direct comparison. The ECMWF IWC at 316 hPa is available but not used because the MLS IWC at 316 hPa is not deemed reliable in current version (v1.5). The spatial distribution of ECMWF UTWV and cloud ice are similar, and each is similar to the MLS measurement (Figure 1 of SU06). A relatively large difference between ECMWF and MLS data occurs over the continental monsoon regions in South America and Central Africa, where ECMWF UTWV and cloud ice are much less than MLS observations. This is likely due to errors in convective parameterization and cloud microphysics over land in the ECMWF assimilation model [*Li et al.*, 2005]. Over the equatorial inter-tropical convergence zones (ITCZ) in the Pacific and Atlantic Oceans, ECMWF has less UTWV but more cloud ice than MLS. This may be related to the model's microphysical scheme. Detailed comparison of MLS and ECMWF cloud ice is presented by *Li et al.* [2005; submitted manuscript, 2006]. Here, we focus on the relationships between UTWV, cloud ice and SST. The approximately linear relations of these quantities are of primary interest.

[6] Figure 2 shows the ECMWF and MLS scatter plots of IWP versus SST, UTWV versus IWP and UTWV versus SST. Only values over tropical oceans from 30°S to 30°N are used. The monthly SST data are from National Centers for Environmental Prediction (NCEP)/National Oceanic and Atmospheric Administration (NOAA) reanalysis, same as in the work by SU06. Different from the scatter plots of SU06 (their Figures 2–4), in which annual means are plotted, Figure 2 uses 12 monthly values from August 2004 to July 2005. Overall, ECMWF and MLS agree with each other quite well. The reason for the differences at low IWP values is because the MLS sensitivity limit prevents obtaining measurements at low IWP [*Livesey et al.*, 2005]. When SST is greater than 300 K, both MLS and ECMWF show that cloud ice increases with increasing SST. In Figures 2a and 2d insets, the increase of cloud ice with SST occurs at similar rate for MLS and ECMWF, with the least squares linear fit slopes of log(IWP) versus SST being 0.71 for MLS and 0.83 for ECMWF. The uncertainties for both linear fits are approximately 5%.

[7] The relationship between UTWV and IWP is shown in Figures 2b and 2e. At the low values of log(IWP) and log(UTWV), where convection is infrequent, the scatter between ECMWF UTWV and IWP is large. Over the convective regions, the two parameters are strongly correlated, with an approximately linear relationship. In these regions, the least squares linear fits to MLS and ECMWF data yield similar slopes: 0.17 and 0.21, respectively, with estimated uncertainties around 2% for each dataset.

[8] In Figures 2c and 2f, MLS and ECMWF UTWV are plotted against SST, with the least squares linear fits shown separately for SST lower than 300 K and greater than 300 K. For both datasets, log(UTWV) increases with SST at 0.07 per degree K when SST is less than 300 K, close to

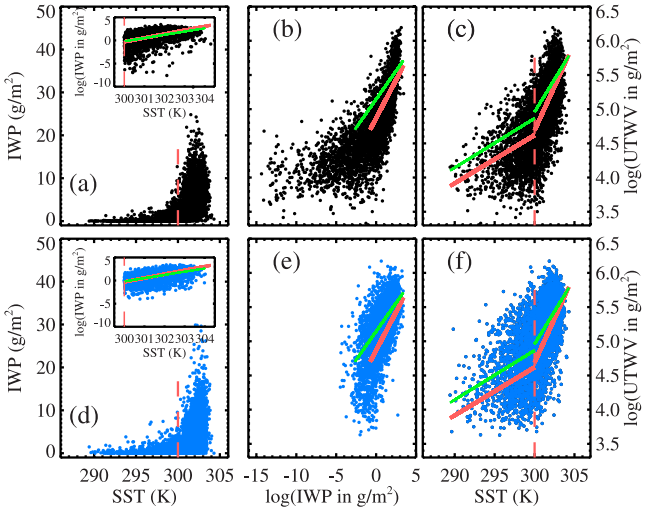

Figure 2. Scatter plot of ECMWF analyses (in black) and MLS-observed (in blue): (a and d) IWP versus SST, (b and e) log(UTWV) (y-axis) versus log(IWP) (x-axis), and (c and f) log(UTWV) (labeled on the right) versus SST. The insets in Figures 2a and 2d show the scatter plot of the log(IWP) versus SST for SST ≥ 300 K. Each point corresponds to a monthly mean from August 2004 to July 2005 in the 8° × 4° oceanic boxes within 30°S–30°N. The red and green lines are the least squares linear fits to the ECMWF and MLS data, respectively, and are repeated in both rows to facilitate comparisons. MLS sensitivity prevents measurements at low values of IWP, which explains the ECMWF and MLS differences at low IWP.

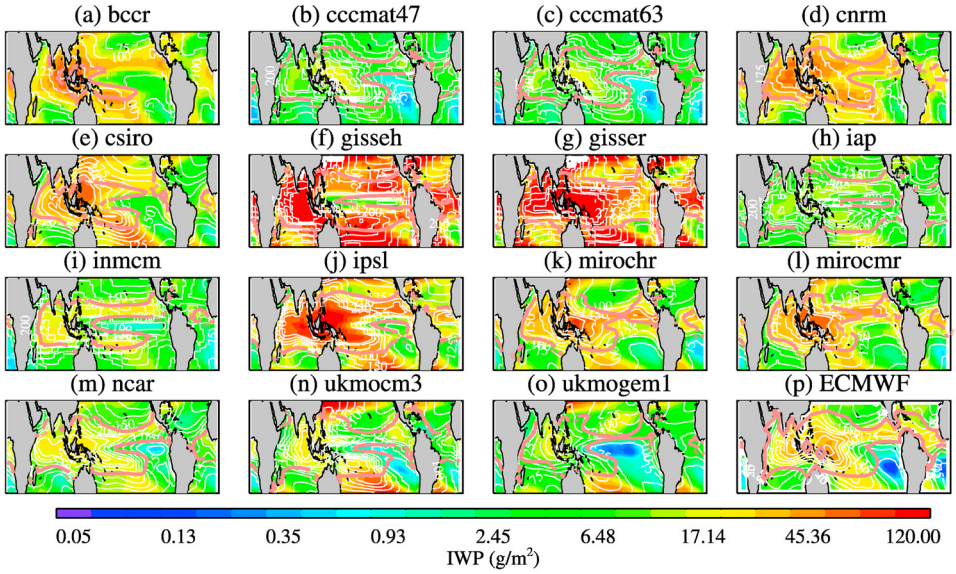

Figure 3. Maps of annual mean tropical (30°S–30°N) UTWV (in white contours), column-integrated IWP (shaded) and SST contour of 300 K (in orange) for the 15 IPCC models and ECMWF analyses. The UTWVs for all panels are contoured at the interval of 25 g m^{-2}.

the theoretical value based on the Clausius-Clapeyon equation. When SST is higher than 300 K, the slopes of log(UTWV) versus SST for MLS and ECMWF are 0.19 and 0.26, respectively, with estimation errors around 5%. The larger sensitivity of ECMWF UTWV to SST than that of MLS may be related to the higher slopes of log(IWP) versus SST and log(UTWV) versus log(IWP) as in Figures 2a, 2d, 2b and 2e. Given the uncertainties in estimated regression slopes, the inferred CWVF, as defined in Equation (1) of SU06, is about 30–45% higher for ECMWF than for MLS.

3. IPCC 20th Century Simulations

[9] To examine the relationships between UTWV, IWP and SST in state-of-the-art GCMs, we analyze the 20th century simulations from 15 coupled atmospheric-ocean GCMs, which were contributed to the IPCC AR4. Here, we use the mean annual cycles averaged for the 30 year period from 1970 to 1999.

[10] For comparison with SU06, the vertical integral of water vapor from 300 hPa to 150 hPa (UTWV) is constructed for all models. The standard outputs of the IPCC runs do not have vertically-resolved IWC. Instead, only tropospheric column-integrated IWP is available. Since most cloud ice occurs in the middle and upper troposphere, the comparison to MLS UT cloud ice is still useful, with a possible scaling factor uncertainty. For reference, ECMWF column-integrated IWP is presented for comparison with the IPCC results, and the UT IWP for MLS and ECMWF. For the analysis of the GCM results, SST simulated from the coupled models is used.

[11] Figure 3 shows the maps of tropical annual-mean UTWV (white contours), column-integrated IWP (shaded), and SST contour of 300 K (in orange) from the IPCC models and ECMWF analyses. All models produce approximately similar distributions of SST, UTWV and IWP in the tropics. The 300 K SST contours encompass approximately the same areas. Relatively large model disagreements occur over the eastern Pacific cold tongue, with some models' 300 K contour extending too far east. For IWP, the magnitudes vary considerably between models, ranging from 20 g m^{-2} to 200 g m^{-2}, excluding the two GISS models, which have a few anomalous points with IWP more than 1000 g m^{-2} near the east coast of Asia around 30°N (shown as the above-scale white areas in Figures 3f and 3g). For references, the maximum column-integrated IWP from ECMWF analyses is 52 g m^{-2}, while the UT (215–147 hPa) IWP for ECMWF and MLS are 12 and 15 g m^{-2}, respectively. Despite the large differences in IWP values, the morphology of IWP is broadly consistent among models. The spatial patterns resemble the tropical convective zones and coincide with the 300 K SST contours. In the subtropics, a few models (e.g., two GISS models and two UKMO models) produce high IWP values, which are not present in ECMWF and MLS observations. The reason for this discrepancy is unknown at present. The distributions of the modeled UTWV are quite similar. The high UTWV occurs over tropical warm oceans and deep convective regions. The maximum values of UTWV vary from 180 to 450 g m^{-2}. The UTWV for ECMWF and MLS are 270 and 310 g m^{-2}, respectively. It is worth noting that the total mass content of cloud ice accounts for only a small fraction (5% - 20%) of UTWV for all models and data. This might suggest that sublimation of detrained cloud ice contributes less to the moistening of UT than the vertical transport of moisture over the deep convective regions. However, the exact contribution of each process to the UT moisture budget cannot be determined solely from the amounts of UTWV and IWP, and a cloud-resolving model combined with observational data is needed to address this issue. Near the margins of convective zones, such as south of the equator in the eastern Pacific, inter-model differences are more conspicuous than over the western Pacific warm pool.

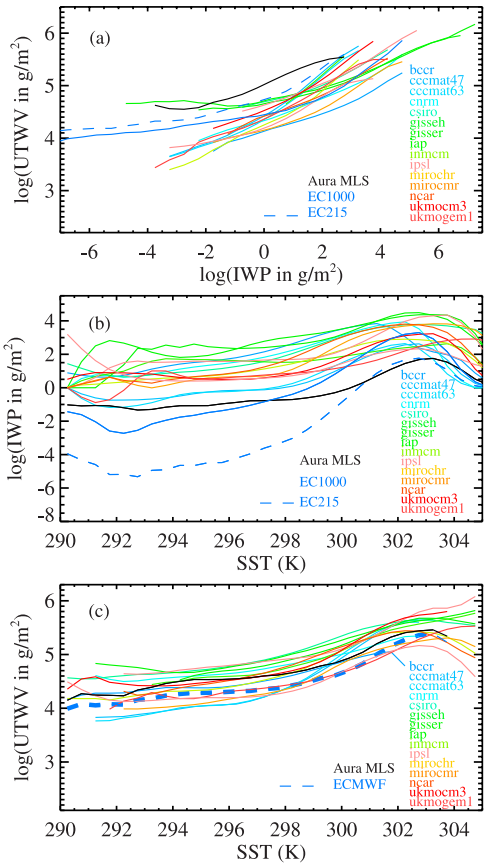

Figure 4. Distributions of (a) log(UTWV) in each 0.5 bin of log(IWP), (b) log(IWP) and (c) log(UTWV) in each 0.5 K bin of SST for the IPCC models along with the ECMWF and MLS. EC215 denotes the UT IWP integrated from 215 hPa to 147 hPa. EC1000 denotes the column-integrated IWP.

The inter-model differences in the magnitudes of maximum IWP and UTWV partially confirm previous findings that climate models better simulate water vapor variations than clouds [e.g., *Held and Soden*, 2000].

[12] The relationships of UTWV, IWP and SST for all models, and for ECMWF and MLS, are shown in Figure 4. The mean annual cycles between 1970 and 1999 are used. Only oceanic grid boxes between 20°S and 20°N are considered, to exclude the spurious high IWP values around 30°N in a few models. In Figure 4a, log(UTWV) is binned on log(IWP) at an interval of 0.5. In Figures 4b and 4c, the modeled IWP and UTWV within each 0.5 K SST bin from 290 to 305 K are displayed. To first order, the positive correlations between log(IWP), log(UTWV) and SST are reproduced in the models, with relatively large scatter in log(IWP) and SST relation (Figure 4b).

[13] The approximately linear relationship between log(UTWV) and log(IWP) is a robust feature for all models (Figure 4a). Since the modeled IWP is over the entire tropospheric column and larger than that for UT IWP (MLS and EC215), the modeled lines roughly shift to the right with respect to MLS and EC215. The regression slopes for all models and data are similar, around 0.2 to 0.4. Figure 5 shows the ratio of the modeled slopes of log(UTWV) versus log(IWP) relative to the MLS-observed (the purple blue bars). The differences between the models and data are within a factor of 2. The ratio for MLS is at the constant of one by definition.

[14] In Figure 4b, IWP stays nearly flat with respect to SST until SST reaches a threshold value, then it increases with SST until another critical point, after which increasing SST is associated with decreasing cloud ice. The threshold SST values for convective initiation vary from model to model, ranging from ~295 K to ~300 K by subjective estimate of the curves in Figure 4b. The critical SST values for peak IWP vary from ~301 K to ~305 K among models. The decrease of cloud ice with increasing SST at high values of SST is consistent with previous studies [e.g., *Waliser et al.*, 1993]. These SST "hot spots" usually develop in subsidence regions. When convection does break out there, it rapidly cools the surface by cloud shortwave radiative effect and increased surface heat fluxes (plus a small contribution from raindrops). The time scale involved in surface warming by subsidence is longer than cooling by convection, resulting in a negative correlation of IWP with SST [*Tompkins*, 2001]. This negative correlation is not obvious in the scatter plots (e.g., Figure 2a) because the number of samples in this high SST range is much smaller than that in lower SST values.

[15] For a quantitative assessment of cloud ice sensitivity to SST in each model, we define the average rate of increase of log(IWP) with SST for individual models as the linear regression slope within 3 K SST range to the left of the SST value at the peak IWP in Figure 4b. The exact magnitude of the slope depends on the range of SST used; however, the ratio between the modeled and the MLS-observed slopes is found to be relatively insensitive to the detailed SST range. Hence, the ratios of modeled regression slopes relative to MLS are displayed in Figure 5 (the cyan bars). All models, except IPSL, produce a smaller rate of increase of IWP with SST, while ECMWF shows a larger rate, consistent with the results in the preceding section. The differences of the ratios among models are approximately by a factor of ~4. Compared to the IWP-SST relation, the log(UTWV) versus SST shows a relatively small divergence between models (Figure 4c). All models show the increase of UTWV with increasing SST at larger rate when SST is higher. The negative correlation of UTWV with SST occurs at high values of SST, corresponding to the negative correlation of IWP with SST there (Figure 4b). Similar to the definition of the average rate of increase of IWP with SST, we use the

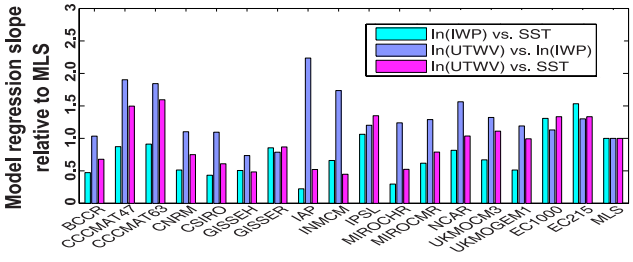

Figure 5. The ratio of the regression slopes of log(IWP)-SST, log(UTWV)-log(IWP), and log(UTWV)-SST relative to the MLS-observed for the IPCC models, ECMWF and MLS.

linear regression slopes of log(UTWV) versus SST within 3 K of the SST below the peak UTWV. The ratio of the modeled log(UTWV)-SST slopes relative to the MLS-observed is shown in Figure 5 (the magenta bars). The ratio varies from 0.5 to 1.5 for the IPCC models, and the ECMWF is about 30–40% larger than the MLS. Overall, the relationships between UTWV, cloud ice and SST are qualitatively captured in these state-of-the-art climate models.

4. Conclusions

[16] It is important to quantify the strength of water vapor feedback for climate change predictions. SU06 used recent satellite observations and found the enhancement of UT water vapor greenhouse effect by tropical deep convection and associated clouds. The strong spatial correlations between UTWV, clouds and SST suggest that deep convection is a primary mechanism for creating the gradient of UTWV across the tropics. For climate models, accurate representation of these spatial relationships in annual cycle is a prerequisite to capture water vapor variations and its response to climate change. Here, the relationships of UTWV, cloud ice and SST are examined in the ECMWF analyses and the IPCC model simulations, and comparisons to the MLS data are presented. The ECMWF analyses agree well with the MLS observations, with about 30% higher sensitivity of IWP and UTWV to SST. For the IPCC 20th century simulations, the magnitudes of IWP vary considerably among models, by nearly a factor of 10. In the model results for IWP versus SST, a non-monotonic relationship is shown. Over most of the tropical oceans where SST exceeds a threshold value around 298–300 K but lower than ~303 K, IWP increases with increasing SST. For very limited regions with SST higher than about ~303 K, IWP decreases with increasing SST, largely due to subsidence warming and reduced surface cooling associated with less convection. The IPCC models differ by a factor of ~4 in terms of the average rate of IWP increase with SST. Because of the coupling of UTWV with IWP, the model UTWV-SST correlations also yield a deviation of approximately a factor of 3. The magnitudes of IWP differ by a factor of 10 among models, while the modeled UTWV differ by a factor of 3. The reasons for the model-data discrepancy are likely due to the shortcomings in the physical parameterizations of clouds in the models; and improvements can be made when coordinated efforts of combined satellite data and model analysis are underway.

[17] We note that the positive correlations between UTWV, IWP and SST are easier to establish in the annual cycle than in other time scales, such as intraseasonal, interannual or long-term trend, since the annual cycle is the most dominant mode of atmospheric internal variability. Whether these relationships are applicable for variabilities on other time scales are yet clear. With the new generation of satellite observations, quantification of regional and global scale water vapor variations is possible. Our analysis is intended to be a starting point for future investigation of UTWV variability, its interaction with upper level clouds, and impacts on climate change.

[18] **Acknowledgments.** This work was carried out at the Jet Propulsion Laboratory, California Institute of Technology, under contract with NASA. We thank C. Zhai for help with the graphics.

References

Betts, A. K. (1990), Greenhouse warming and the tropical water budget, *Bull. Am. Meteorol. Soc.*, *71*, 1464–1465.

Held, I. M., and B. J. Soden (2000), Water vapor feedback and global warming, *Annu. Rev. Energy Environ.*, *25*, 441–475.

Li, J.-L., et al. (2005), Comparisons of EOS MLS cloud ice measurements with ECMWF analyses and GCM simulations: Initial results, *Geophys. Res. Lett.*, *32*, L18710, doi:10.1029/2005GL023788.

Lindzen, R. S. (1990), Some coolness concerning global warming, *Bull. Am. Meteorol. Soc.*, *71*, 288–299.

Livesey, N. J., et al. (2005), EOS MLS version V1.5 level 2 data quality and description document, Jet Propul. Lab., Pasadena, Calif. (Available at http://mls.jpl.nasa.gov.)

Pierrehumbert, R. H. (2002), The hydrologic cycle in deep time climate problems, *Nature*, *419*, 191–198.

Raval, A., and V. Ramanathan (1989), Observational determination of the greenhouse effect, *Nature*, *342*, 758–762.

Soden, B. J., and R. Fu (1995), A satellite analysis of deep convection, upper-tropospheric humidity, and the greenhouse effect, *J. Clim.*, *8*, 2333–2351.

Su, H., W. G. Read, J. H. Jiang, J. W. Waters, D. L. Wu, and E. J. Fetzer (2006), Enhanced positive water vapor feedback associated with tropical deep convection: New evidence from Aura MLS, *Geophys. Res. Lett.*, *33*, L05709, doi:10.1029/2005GL025505.

Sun, D. Z., and R. S. Lindzen (1993), Distribution of tropical tropospheric water vapor, *J. Atmos. Sci.*, *50*, 1644–1660.

Tompkins, A. M. (2001), On the relationship between tropical convection and sea surface temperature, *J. Clim.*, *14*, 633–637.

Tompkins, A. M., and G. C. Craig (1999), Sensitivity of tropical convection to sea surface temperature in the absence of large-scale flow, *J. Clim.*, *12*, 462–476.

Udelhofen, P. M., and D. L. Hartmann (1995), Influence of tropical cloud systems on the relative humidity in the upper troposphere, *J. Geophys. Res.*, *100*, 7423–7440.

Waliser, D. E., N. E. Graham, and C. Gautier (1993), Comparison of the highly reflective cloud and outgoing longwave radiation datasets for use in estimating tropical deep convection, *J. Clim.*, *6*, 331–353.

Waters, J. W., et al. (2006), The Earth Observing System Microwave Limb Sounder (EOS MLS) on the Aura satellite, *IEEE Trans. Geosci. Remote Sens.*, *44*, 1075–1092.

J. H. Jiang, J. Li, W. G. Read, H. Su, D. E. Waliser, and J. W. Waters, Jet Propulsion Laboratory, California Institute of Technology, Pasadena, CA 91109, USA. (hui.su@jpl.nasa.gov)

A. M. Tompkins, European Center for Medium-Range Weather Forecasts, Shinfield Park, Reading RG1 1NT, UK.